

Reaction dynamic dependences of (^{16}O , ^{15}N) small angle cross sections*

J. V. Maher, J. C. Peng, D. A. Sink, C. M. Cheng, H. S. Song, and T. J. Lewis

University of Pittsburgh, Pittsburgh, Pennsylvania 15260

(Received 18 June 1976)

Angular distributions have been measured for angles $\theta_{\text{lab}} \geq 4^\circ$ for (^{16}O , ^{15}N) transitions on $2s$ - $1d$ and $1f$ - $2p$ shell targets at bombarding energies $36 \leq E_{\text{lab}} \leq 53$ MeV. More than one transition has been studied for each l value from 1 through 4 and the transition Q values vary from nearly optimum to severely unfavored. A full-finite-range distorted-wave Born approximation analysis is successful in reproducing angular distribution shapes for transitions with bombarding energies well above the entrance channel Coulomb barrier, but such an analysis fails badly to fit angular distributions for lower bombarding energies, especially for unfavored Q value transitions. There is some variation of the extracted absolute spectroscopic factors with bombarding energy, but in general the spectroscopic factors are in good agreement with (^3He , d) results if the distorted-wave Born approximation predictions are normalized to the experimental cross sections at the grazing angle. The relative cross section contributions to the full distorted-wave Born approximation calculation from different m substates are strongly dependent on Q value and on small changes in optical potential parameters; the failures in the distorted-wave Born approximation analysis may arise from a miscalculation of the nuclear alignment.

[NUCLEAR REACTIONS ^{26}Mg , ^{27}Al , $^{48,50}\text{Ti}$, ^{56}Fe , ^{62}Ni (^{16}O , ^{15}N); measured $\sigma(E, \theta)$; DWBA analysis; enriched targets; $36 \text{ MeV} \leq E \leq 53 \text{ MeV}$.]

I. INTRODUCTION

Since the original report of large cross sections at small angles in angular distributions for heavy-ion-induced transfer reactions,¹ many investigators have addressed themselves to exploring the extent of the phenomenon and studying the mechanism which produces such cross sections.²⁻⁵ This, along with the general availability of full-finite-range distorted-wave Born approximation (DWBA) codes,^{6,7} has also led to reinvestigation of other previously noted^{8,9} features of heavy-ion-induced transfer cross sections. A recent report on the $^{24}\text{Mg}({}^{16}\text{O}, {}^{12}\text{C})$ and $^{28}\text{Si}({}^{16}\text{O}, {}^{12}\text{C})$ reactions has indicated a sensitivity to choice of optical potential of the shape of the DWBA-predicted angular distributions which becomes progressively more severe as bombarding energy is reduced toward the Coulomb barrier.³ The same study reports a factor of ~ 5 change in absolute spectroscopic factor as beam energy is varied by ~ 20 MeV, while relative spectroscopic factors are energy independent and agree well with (^6Li , d) results. A similar discrepancy in absolute spectroscopic factor has also been reported for the $^{26}\text{Mg}({}^{16}\text{O}, {}^{14}\text{C})$ reaction.¹⁰

While multinucleon transfer reactions with heavy ions are spectroscopically more interesting, single-nucleon transfer reactions like (^{16}O , ^{15}N) should provide a better test of reaction mechanism effects since well understood analogous reactions exist [e.g., (^3He , d)] and dynamical and structure features of the DWBA calculations are more readily separated. Single-nucleon transfer data have

provided a very rich variety of angular distribution shapes, but unfortunately for attempts to compare different transitions, calculations of such cross sections appear to be quite sensitive to several quantities, the most important of which are (1) the strength of absorption in the optical potentials, where less absorption generally increases the small angle cross sections and (2) the Q values of the reaction, where a poor match in momentum and/or angular momentum can result in small, roughly equal reaction contributions from many entrance channel partial waves, which in turn tends to wash out any structure in the DWBA angular distribution other than the broad grazing angle maximum ("bell shape"). Further, there is evidence that DWBA predictions of the relative population of various m (projection of orbital angular momentum transfer, l , on the beam axis) substates may under some conditions be unphysical; such an effect has been argued to produce angle shifted oscillations for $^{40}\text{Ca}({}^{13}\text{C}, {}^{14}\text{N})$ angular distributions.¹¹

In the present work, angular distributions (laboratory angle, $\theta_{\text{lab}} \geq 4^\circ$) have been measured for (^{16}O , ^{15}N) transitions on a variety of $2s$ - $1d$ and $1f$ - $2p$ shell targets at a variety of bombarding energies. The Q values of the transitions range from nearly optimum to ~ 5 MeV more negative than optimum, and more than one transition is observed for each l value from 1 to 4. An extensive series of full-finite-range DWBA calculations has been performed to investigate the ability of such calculations to reproduce the measured cross sections, their sensitivity to parameter variations,

and the contributions of different m substates to the predicted cross sections.

II. EXPERIMENTAL ARRANGEMENT AND DATA PRESENTATION

The University of Pittsburgh three stage Van de Graaff accelerator was used to provide 6^+ and 7^+ beams of ^{16}O at laboratory energies from 36 to 53 MeV to induce ($^{16}\text{O}, ^{15}\text{N}$) transitions on $\sim 35 \mu\text{g}/\text{cm}^2$ targets of ^{26}Mg (Mg metal enriched to $>99\%$ in ^{26}Mg), ^{27}Al , $^{48,50}\text{Ti}$ (Ti O_2 enriched to >99 and 75% in ^{48}Ti and ^{50}Ti , respectively), ^{56}Fe (natural abundance Fe_2O_3) and ^{62}Ni (NiO enriched to $>98\%$). All but the Al targets had $20 \mu\text{g}/\text{cm}^2$ C backings. Emerging ^{15}N ions were detected with an array of up to four, 5 cm long Au-Si triode position sensitive detectors (PSD's) placed in the focal plane of a split-pole spectrograph. The spectrograph entrance aperture subtended a solid angle of 1.7 msr. Initially both 6^+ and 7^+ ^{15}N groups were detected, but the yield ratios of these charge states proved quite reproducible at vacuums typical for the spectrograph and scattering chamber ($\sim 2 \times 10^{-6}$ Torr) so only the dominant 7^+ ion groups were measured during the later phases of this experiment. The PSD's were positioned in the focal plane to detect particle groups corresponding to transitions known from previous ($^3\text{He}, d$) and/or ($^{16}\text{O}, ^{15}\text{N}$) studies to have large proton transfer spectroscopic factors. Normally all interesting particle groups could be measured at once, but for a few combinations of angle, beam energy, and target, it was necessary to use two different magnetic field settings. E (energy) and Ex (position times energy) signals from the PSD's were digitized in a PACE

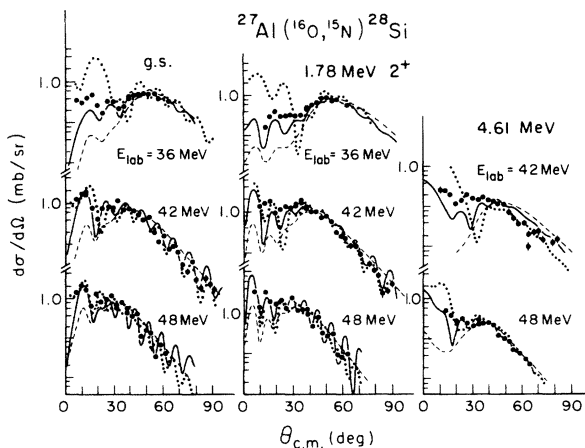


FIG. 1. Angular distributions for $^{27}\text{Al} \rightarrow ^{28}\text{Si}$ transitions. Errors from counting statistics are indicated. The curves result from the DWBA calculations discussed in the text.

IV analog-to-digital system and stored in four two-dimensional (128×32) arrays in the on-line processor of the laboratory's dual PDP 15 computer system. A monitor detector (Au-Si diode) was placed at a laboratory angle of 34° . For all targets the elastic scattering cross section at this angle was a large fraction of the Rutherford cross section and optical model predictions of this fraction were rather insensitive to changes in optical model parameters. The absolute cross sections for ($^{16}\text{O}, ^{15}\text{N}$) transitions were established from target thicknesses determined by the elastic yield in the monitor detector. The error in absolute cross sections should be considerably less than 20%.

Figures 1-4 show the ($^{16}\text{O}, ^{15}\text{N}$) angular distributions measured in this investigation. In several cases [all $^{27}\text{Al} \rightarrow ^{28}\text{Si}$ transitions⁹; both $^{26}\text{Mg} \rightarrow ^{27}\text{Al}$ transitions at 42 MeV (Ref. 12) and the $^{48}\text{Ti} \rightarrow ^{49}\text{V}$ and $^{50}\text{Ti} \rightarrow ^{51}\text{V}$ transitions at 48 MeV (Refs. 8 and 9)] angular distributions had already been measured with Si detector telescopes at large angles ($\theta_{\text{lab}} \geq 22^\circ$). These previously published data are included in Figs. 1-4. Figure 2 also includes angular distributions for $^{26}\text{Mg} \rightarrow ^{27}\text{Al}$ transitions measured at a bombarding energy of 45 MeV and reported in Ref. 2. (These and the large angle data of the angular distribution for the transition to the 2.41 MeV state of ^{51}V are indicated with crosses in Figs. 2 and 4 to indicate that they were not measured in the Pittsburgh laboratory.) The absolute cross sections of the previously published data always agreed within $\sim 10\%$ with those established in this experiment.

The angular distributions shown in Figs. 1-4 exhibit a wide range of shapes, varying from oscillatory (e.g., the $^{27}\text{Al} \rightarrow ^{28}\text{Si}$ ground state transition at 48 MeV) to bell shaped at angles characteristic of a grazing collision with or without pronounced small angle structure (e.g., the $^{48}\text{Ti} \rightarrow ^{49}\text{V}$ ground state transitions and the transitions to excited states of $^{49,51}\text{V}$).

III. DWBA ANALYSIS AND DISCUSSION

A. Parameters of the calculations

All DWBA calculations presented herein are exact finite-range calculations performed with the code LOLA.¹³ Form factors representing the wave function of the transferred proton bound to an ^{15}N core (to form the ^{16}O projectile) and bound to the target (to form the residual nuclide) were calculated by varying the well depth of a Woods-Saxon potential to produce the correct binding energy for the relevant nuclear state; the nuclear and Coulomb radius parameters of this binding well were set at 1.20 fm and its diffuseness was 0.65 fm.

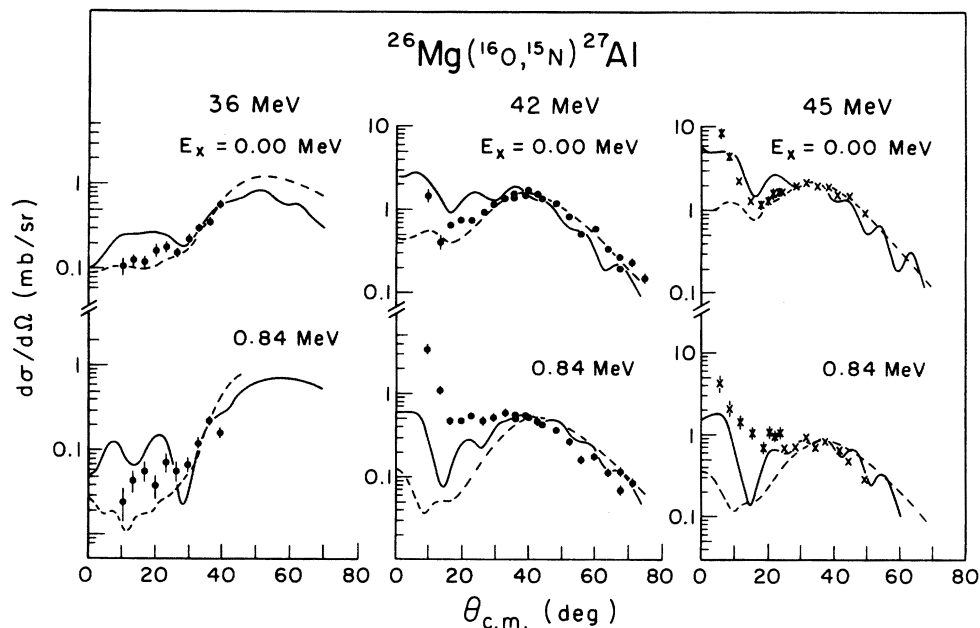


FIG. 2. Angular distributions for $^{26}\text{Mg} \rightarrow ^{27}\text{Al}$ transitions. Errors from counting statistics are indicated. The curves result from the DWBA calculations discussed in the text. The data points shown as \times 's have been taken from Ref. 2.

Changing the radius of the binding well to 1.25 fm typically increased the absolute cross section of the DWBA prediction by $\sim 40\%$; however, such a change did not affect the shape of the predicted angular distribution nor did it affect the beam energy dependence of the absolute DWBA cross section. Calculations were performed which included Coulomb terms in the DWBA interaction potential; inclusion of these terms also affected the predicted absolute cross sections (decreasing them by

$\sim 20\%$) but changed neither the shapes of the angular distributions nor the beam energy dependence of the absolute cross sections. The results presented below were extracted with calculations which did not include the Coulomb terms in the interaction potential. All calculations presented below were performed with the post representation of the DWBA amplitude. (A more extensive discussion of the above considerations is contained in Ref. 3.)

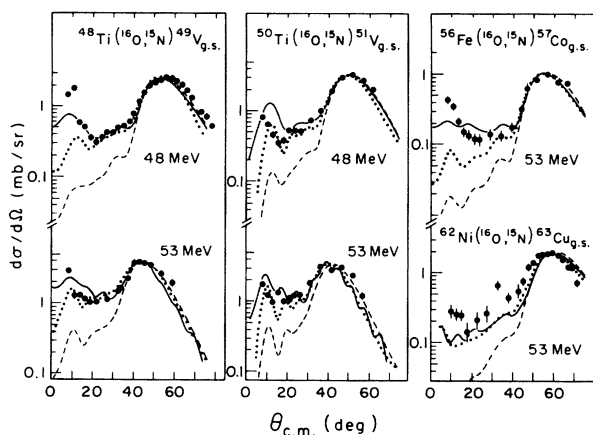


FIG. 3. Angular distributions for transitions populating the ground states of $1f-2p$ shell nuclides. Errors from counting statistics are indicated. The curves result from the DWBA calculations discussed in the text.

B. Choice of optical potentials

Extensive data exist for ^{16}O and ^{15}N scattering on Mg and Si isotopes and analysis of these data has yielded shallow depths for both the real and imaginary parts of the best fit optical potentials.¹⁴ DWBA calculations which employ these transparent potentials show unphysical reaction contributions from the deep nuclear interior (e.g., introduction of a radial cutoff of 3 fm or more to the DWBA integral for an $^{27}\text{Al} \rightarrow ^{28}\text{Si}$ ground state calculation changed both the shape and the absolute cross section of the predicted angular distribution while the center to center separation at which the undisturbed $^{16}\text{O} + ^{27}\text{Al}$ system reaches normal nuclear density is ~ 6 fm). For this reason these potentials were not used in earlier analyses of (^{16}O , ^{15}N) reaction data^{8,9} although it was noted⁹ that oscillations in $^{27}\text{Al}(^{16}\text{O}, ^{15}\text{N})^{28}\text{Si}$ angular distributions were not reproduced by DWBA calculations which em-

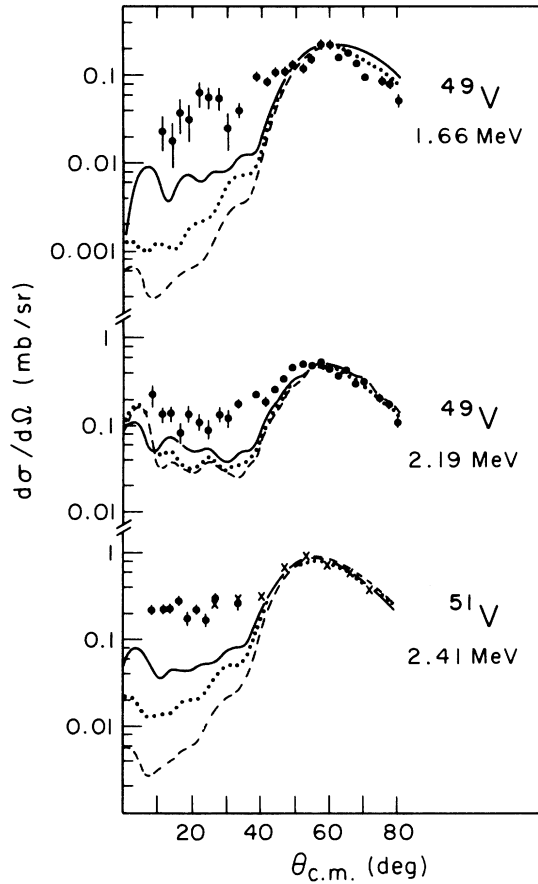


FIG. 4. Angular distributions for transitions populating excited states of ^{49}V and ^{51}V . Errors from counting statistics are indicated. The data points shown as \times 's have been taken from Ref. 8. The curves result from the DWBA calculations discussed in the text.

ployed strongly absorbing potentials.

Elastic scattering data for ^{16}O on $1f$ - $2p$ shell targets are scarce, and for ^{15}N scattering, data are not available. Such data as exist exhibit gross strong absorption features that are rather easily predicted with any of a wide range of optical potential parameter sets. Some of the ambiguities can be lifted by requiring the optical potential prediction to fit the fine details of the elastic scattering angular distributions.¹⁵ However, it is still possible to construct phase equivalent potentials which predict virtually identical elastic scattering cross sections while retaining significant differences in S matrix elements that strongly effect the DWBA predictions for transfer reaction channels. To generate optical potentials for the present analysis the elastic scattering angular distributions^{9, 16} shown in Fig. 5 were fitted¹⁷ with several qualitatively different Woods-Saxon optical potentials. Three of these potential sets are listed in Table I.

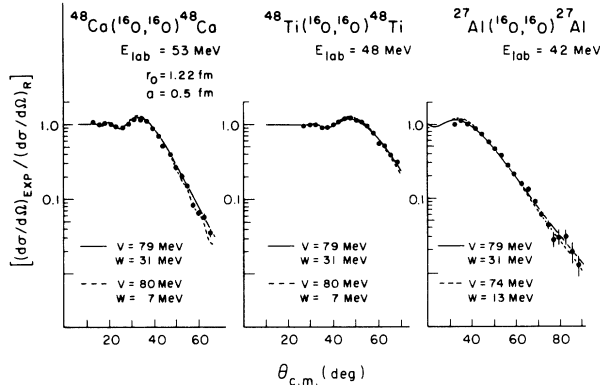


FIG. 5. Angular distributions for elastic scattering of ^{16}O from ^{27}Al , ^{48}Ca , and ^{48}Ti . The solid curves result from optical model calculations with potential A of Table I. The dashed curves result from optical model calculations with drastically weakened absorption as discussed in the text.

Potential sets A and B are four parameter sets which use a Woods-Saxon geometry introduced by Voos *et al.* to analyze heavy-ion-induced transfer reactions on $1p$ shell targets¹⁸ and used until recently for most of the analyses of (^{16}O , ^{15}N) reactions. Set A represents the best fit with this geometry — a strongly absorbing potential which yields the cross sections shown as solid curves in Fig. 5. Cross sections predicted by potential set A were found to be very insensitive to changes in W , the imaginary well depth; e.g., for the $1f$ - $2p$ shell targets, W could be reduced from 31 to ~ 7 MeV before χ^2 , the sum of squares of deviations, became double the best fit value. The dashed curves in Fig. 5 result from calculations with the value of W which yields a χ^2 double the best fit value. Thus potential set B of Table I accounts for the elastic scattering data almost as well as does potential A even though potential B is considerably less absorptive. Potential set C of Table I is a six parameter potential which sets the imaginary radius and diffuseness smaller than those of the real well to combine transparency near the nuclear surface with strong absorption in the nuclear interior.¹⁹ (Potential set C fits the data of Fig. 5 as well as does either of Sets A and B, but its cross section predictions are not shown in Fig. 5.) Set C is closely related to the set which gave the best fit to the beam energy dependence of $^{24}\text{Mg}(^{16}\text{O}, ^{12}\text{C})$ and $^{28}\text{Si}(^{16}\text{O}, ^{12}\text{C})$ reaction data.³

In the reaction calculations discussed below, the ^{15}N optical potential parameters were, except where otherwise specified, set equal to those of the ^{16}O potential. It is unfortunate that more is not known about ^{15}N scattering, particularly be-

TABLE I. Optical potential parameters used in the DWBA analysis discussed in the text. All potential sets use Woods-Saxon shape. Except as indicated in the text, ^{15}N potential parameters were assumed to be identical to corresponding ^{16}O potentials.

Potential set	V (MeV)	r_v (fm)	r_{Coul} (fm)	a_v (fm)	W (MeV)	r_w (fm)	a_w (fm)
A	79	1.22	1.22	0.5	31	1.22	0.5
B	80	1.22	1.22	0.5	10	1.22	0.5
C	30.8	1.307	1.307	0.493	6.67	1.242	0.204

$$R_{v,w} = r_{v,w}(A_1^{1/3} + A_2^{1/3}), \quad U(r) = \frac{-V}{1 + \exp[(r - R_v)/a_v]} - \frac{iW}{1 + \exp[(r - R_w)/a_w]}$$

cause of the evidence discussed below that the DWBA angular distribution shapes are very sensitive to changes in exit channel optical parameters.

C. Angular distribution shapes

The curves shown with the data in Figs. 1–4 result from DWBA calculations which use optical potential sets A (dashed curves), B (dotted curves in Figs. 3 and 4), and C (solid curves). None of these sets of calculations gives a generally good account of the data and the most striking failures occur at small angles where the calculations generally underestimate the cross sections. Table II lists Q values and orbital angular momentum transfers (l) for all transitions studied in this investigation. As is discussed below, DWBA calculations appear to succeed more easily in fitting small angle reaction cross sections if the Q value is near the optimum value for momentum and angular momentum matching. To facilitate the Q value discussion, Table II also lists several approximate optimum Q values calculated with the relation

$$Q_{\text{opt}} = \left(\frac{Z_3 Z_4}{Z_1 Z_2} - 1 \right) E_{\text{c.m.}},$$

where $Z_{3,4}$ ($Z_{1,2}$) are the atomic numbers of the exit (entrance) channel nuclides and $E_{\text{c.m.}}$ is the center of mass energy in the entrance channel.²⁰ (While there are more sophisticated formulations,²¹ this simple formula seems adequate to the present discussion.)

Both (^{16}O , ^{12}C) angular distributions and those presented here for the (^{16}O , ^{15}N) reaction appear to become more difficult to fit with DWBA calculations if the bombarding energy is reduced toward the Coulomb barrier. In the (^{16}O , ^{12}C) case this trend is clearer because most reasonable optical potentials can be used successfully in DWBA calculations for beam energies ~ 15 MeV above the Coulomb barrier, but only a surface transparent potential like potential C can be used near the

barrier.³ The situation with the (^{16}O , ^{15}N) results presented here is less clear because no DWBA calculation has fitted the bulk of the data and calculations for even the very well matched $^{27}\text{Al} - ^{28}\text{Si}$ ground state transition at the highest bombarding energy are quite sensitive to choice of optical potential. Table II also includes a rough estimate of the laboratory kinetic energy needed to surpass the Coulomb barrier for several entrance channels. The barrier has been calculated to be $E_B = KZ_1 Z_2 / 1.25 (A_1^{1/3} + A_2^{1/3})$ where Z_i, A_i are the charge and mass number of the i th particle and K has been adjusted to place the $^{27}\text{Al} + ^{16}\text{O}$ Coulomb barrier at a laboratory energy of 35 MeV. [The $^{27}\text{Al} (^{16}\text{O}, ^{15}\text{N}) ^{28}\text{Si}$ cross sections are known to decrease sharply below 35 MeV.²²]

I. $^{27}\text{Al} (^{16}\text{O}, ^{15}\text{N}) ^{28}\text{Si}$ transitions

For the $^{27}\text{Al} (^{16}\text{O}, ^{15}\text{N}) ^{28}\text{Si}$ transitions, the calculations with potential set C are clearly the most successful. These calculations reproduce the periodicity of the ground state angular distributions at all beam energies and fail to reproduce the small angle maximum cross sections only at the lowest bombarding energy. This $l = 3$ ground state transition has a very favorable Q value of -0.543 MeV. ($l = 2$ is also allowed since a $1p_{1/2}$ proton is transferred to a $1d_{5/2}$ orbital, but $l = 2$ contributions to the DWBA predictions are negligible.) The failure to fit the envelope of the data only at the lowest beam energy is reminiscent of the Mg, Si- (^{16}O , ^{12}C) reaction cross sections where fitting with DWBA angular distributions became qualitatively more difficult as beam energy was reduced toward the Coulomb barrier. The $l = 1$ transition ($1p_{1/2} - 2s_{1/2}$) to the 2^+ state at 1.78 MeV in ^{28}Si also has a nearly optimum Q value but is less well fitted than is the ground state transition. However, the calculation with potential set C is quite consistent with the highest energy (48 MeV) data. The transition to the 4.61 MeV 4^+ state of ^{28}Si is reasonably well fitted at 48 MeV but at 42 MeV its

TABLE II. Spectroscopic and reaction dynamic information for transitions investigated in this work.

	E_x (MeV)	Q (MeV)	l	Assumed configuration	$E_{\text{beam, lab}}$ (MeV)	$\frac{2J_f+1}{2J_i+1} C^2S$			$(^3\text{He}, d)$
						$(^{16}\text{O}, ^{15}\text{N})$ Potential A	$(^{16}\text{O}, ^{15}\text{N})$ Potential B	$(^{16}\text{O}, ^{15}\text{N})$ Potential C	
$^{26}\text{Mg} \rightarrow ^{27}\text{Al}^{\text{a}}$ ($E_B^{\text{b}} \approx 32$ MeV; $Q_{\text{opt}} \approx -1.3$ MeV)	0.00	-3.9	3	$1d_{5/2}$	36	1.9		1.2	1.5
					42	1.9	1.5		
	0.84	-4.7	1	$2s_{1/2}$	36	4.5		2.8	1.0
					42	0.82	0.85		
					45	0.98	0.85		
$^{27}\text{Al} \rightarrow ^{28}\text{Si}^{\text{c}}$ ($E_B \approx 35$ MeV; $Q_{\text{opt}} \approx -1.5$ MeV)	0.00	-0.5	3	$1d_{5/2}$	36	0.85		0.75	0.44
					42	1.0	1.0		
					48	0.75	0.48		
	1.78	-2.3	1	$2s_{1/2}$	36	0.60		0.48	0.38
					42	0.50	0.53		
					48	0.60	0.60		
4.62	-5.1	1(+2)	$1d_{3/2}$	42	1.2		1.1	0.32	
				48	1.1	1.0			
$^{48}\text{Ti} \rightarrow ^{49}\text{V}^{\text{d}}$ ($E_B \approx 53$ MeV; $Q_{\text{opt}} \approx -3.2$ MeV)	0.00	-5.4	4	$1f_{7/2}$	48	7.9	7.0	5.4	2.5, 4.3
					53	9.0	8.0	5.5	
	1.66	-7.0	2	$2p_{3/2}$	48	0.8	0.6	0.6	0.38, 0.50
					2.19	-7.6	2	$1f_{5/2}$	
$^{50}\text{Ti} \rightarrow ^{51}\text{V}^{\text{e}}$	0.00	-4.1	4	$1f_{7/2}$	48	9.2	6.7	5.5	5.6, 6.0
					53	8.5	6.2	4.4	
	2.41	-6.5	2	$2p_{3/2}$	48	2.1	1.8	1.5	1.7, 2.3, 1.8, 2.6
$^{56}\text{Fe} \rightarrow ^{57}\text{Co}^{\text{f}}$	0.00	-6.1	4	$1f_{7/2}$	53	2.6	1.9	1.9	1.8
$^{62}\text{Ni} \rightarrow ^{63}\text{Cu}^{\text{g}}$	0.00	-6.0	2	$2p_{3/2}$	53	2.1	1.6	1.7	2.6, 3.1

^a($^3\text{He}, d$) information and configurations from H. F. Lutz, D. W. Heikkinen, W. Bertolini, and T. H. Curtis, Phys. Rev. C **2**, 981 (1970).

^bApproximate Coulomb barrier in entrance channel in laboratory frame.

^c($^3\text{He}, d$) information and configuration assumptions from reference 22.

^d($^3\text{He}, d$) information and configuration assumptions from D. J. Pullen, B. Rosner, and O. Hansen, Phys. Rev. **166**, 1142 (1968); D. Bachner, R. Santo, H. H. Duham, R. Bock and S. Hinds, Nucl. Phys. **A106**, 577 (1968).

^e($^3\text{He}, d$) information and configuration assumptions from D. J. Pullen, B. Rosner, and O. Hansen, Phys. Rev. **177**, 1568 (1969); B. Cujec and I. M. Szogky, *ibid.* **179**, 1060 (1969); B. J. O'Brien, W. E. Dorenbusch, T. A. Belote, and J. Rapaport, Nucl. Phys. **A104**, 609 (1967); C. St. Pierre, P. N. Maheshwari, D. Doutriaux, and L. Lamarche, *ibid.* **A102**, 433 (1967).

^f($^3\text{He}, d$) information from B. Rosner and C. H. Holbrow, Phys. Rev. **154**, 1080 (1967).

^g($^3\text{He}, d$) information from D. L. Smith, H. Y. Chen, and H. A. Enge, Nucl. Phys. **A107**, 639 (1968); A. G. Blair, Phys. Rev. **140**, B648 (1965).

shape is quite poorly reproduced over the entire angular range. This transition (presumed²³ to be $1p_{1/2} \rightarrow 1d_{3/2}$ and thus $l = 1$ with an $\sim 15\%$ $l = 2$ admixture) has an unfavorable Q value of -5.15 MeV.

Despite the difficulty discussed above of spurious contributions from the deep nuclear interior, DWBA calculations were performed using the very transparent optical potentials of Siemssen *et al.* (The $^{16}\text{O} + ^{26}\text{Mg}$ potential parameters were used in the entrance channel and the $^{15}\text{N} + ^{28}\text{Si}$ potential was used for the exit channel.¹⁴) The resulting cross sections are shown as dotted curves in Fig. 1. Whereas all the other DWBA curves shown in Figs. 1-4 were individually normalized to fit the data, these have been adjusted to fit the 48 MeV data and

required to yield the same spectroscopic factors (discussed below) at the lower beam energies. While the interference patterns are more strongly fluctuating for these calculations and the overall fit is somewhat poorer, they are qualitatively quite similar to those performed with the surface transparent potential C. For a discussion of the distribution in exit channel partial waves of contributions (β_{lm}^T) to DWBA calculations using these potentials, see Ref. 3.

2. $^{26}\text{Mg}(^{16}\text{O}, ^{15}\text{N})^{27}\text{Al}$ transitions

As can be seen in Fig. 2, the $^{26}\text{Mg} \rightarrow ^{27}\text{Al}$ angular distributions bear considerably less resemblance

to the DWBA predictions than do the $^{27}\text{Al} \rightarrow ^{28}\text{Si}$ angular distributions discussed above. The $l=3$ ($1p_{1/2} \rightarrow 1d_{5/2}$) ground state transition has a rather unfavorable Q value (-3.9 MeV) and the $l=1$ ($1p_{1/2} \rightarrow 2s_{1/2}$) transition to the $J^\pi = \frac{1}{2}^+$ state at 0.84 MeV is more severely mismatched. Calculations with potential set A badly underestimate the small angle cross sections at the higher beam energies. Calculations using potential C oscillate more than the data warrant and fail miserably to reproduce the shapes of the $l=1$ angular distributions. At 60 MeV both $^{27}\text{Al} \rightarrow ^{28}\text{Si}$ and $^{26}\text{Mg} \rightarrow ^{27}\text{Al}$ transitions have been seen² to be rather easily fitted with DWBA calculations. This suggests that the (^{16}O , ^{15}N) transitions, like (^{16}O , ^{12}C), do become more sensitive to choice of parameters — or to reaction mechanism assumptions — near the Coulomb barrier and that this sensitivity is heightened for transitions with unfavorable Q values.

3. Transitions involving $1f$ - $2p$ shell nuclides

The angular distributions shown in Fig. 3 all correspond to transitions which populate the ground states of residual nuclides. The $^{48,50}\text{Ti} \rightarrow ^{49,51}\text{V}$ and $^{56}\text{Fe} \rightarrow ^{57}\text{Co}$ transitions are somewhat mismatched with $l=4$ ($1p_{1/2} \rightarrow 1f_{7/2}$) and Q values from -4 to -6 MeV. The $^{62}\text{Ni} \rightarrow ^{63}\text{Cu}$ transition is $l=2$ ($1p_{1/2} \rightarrow 2p_{3/2}$) with $Q = -6$ MeV and so is more severely mismatched. As was the case for the $2s$ - $1d$ shell transitions discussed above, calculations which use the strongly absorbing potential set A severely underestimate the small angle cross sections for all transitions. Calculations using the more transparent potentials B and C show small angle cross sections in better, but generally not good, agreement with the data.

In an effort to isolate and understand the effects of Q value and absorption on the reaction calculations a series of calculations was run in which Q or the imaginary well depths were arbitrarily displaced from their correct values. In Fig. 6 calculations with potential set B are shown for Q values displaced by ± 2 and $+4$ MeV from the correct value for each of the $1f$ - $2p$ ground state transitions. It is clear that the DWBA can produce a small angle peak (of the sort exhibited by all the $l=4$ data) for Q values near the optimum value of ~ -3 MeV. This was also seen for the very well matched $^{48}\text{Ca}(^{16}\text{O}, ^{15}\text{N})^{49}\text{Sc}$ ground state transition at bombarding energies of 56 MeV (Ref. 2) and 53 MeV (Ref. 16) where DWBA calculations provided excellent fits even though the angular distributions were quite similar to that of the 48 MeV $^{48}\text{Ti}(^{16}\text{O}, ^{15}\text{N})^{49}\text{V}$ ground state angular distribution reported herein. On the other hand, arbitrary Q value displacements do not bring the DWBA calculations into any detailed agreement with the data.

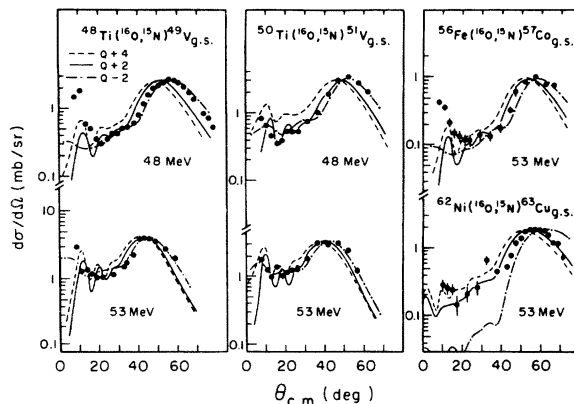


FIG. 6. The Q dependence of DWBA calculations: The data of Fig. 3 are shown with DWBA calculations which differ from the dotted curves of Fig. 3 in the Q value assumed for the transition.

Figure 7 shows calculations with potential set B for the $1f$ - $2p$ shell ground state transitions where the imaginary well depths, W , in both entrance and exit channels were arbitrarily reduced from 10 MeV to 7 and 5 MeV. While this reduction of W certainly enhances the small angle cross sections, it also washes out the valley which normally appears between the grazing angle and small angle maximum cross sections. While absorption clearly plays a role^{1,24} in allowing large cross sections at small angles and potentials with surface transparency are probably the best to use in DWBA calculations, reduced absorption alone cannot account for the experimental situation. Baltz *et al.* have suggested a need for an optical potential which combines a strong, short-range volume imaginary part with a relatively weak surface de-

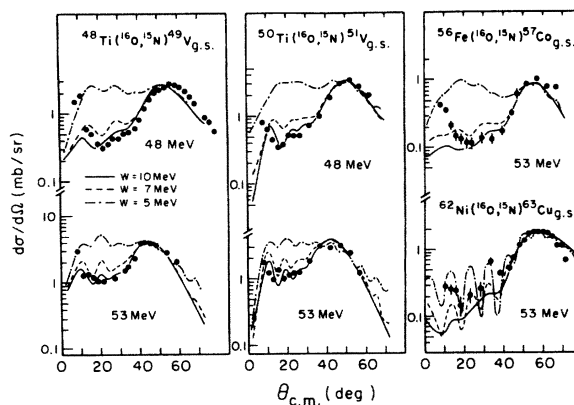


FIG. 7. Absorption (W) dependence of DWBA calculations: The data of Fig. 3 are shown with DWBA calculations which differ from the dotted curves of Fig. 3 in the depth of the imaginary potential assumed for both entrance and exit channels.

rivative absorptive potential.²⁴ Such a potential was adjusted to fit the elastic scattering data of Fig. 5, but when this potential was used in DWBA calculations the resulting angular distributions were generally inferior to the calculations shown in Figs. 1-4.

The angular distributions for transitions populating ^{49,51}V excited states (Fig. 4) have much less pronounced small angle structure than do the ground state angular distributions. Even though all three transitions are $l=2$ (with all the DWBA calculations predicting negligible contributions from the other allowed l value, 1 or 3), the DWBA calculations predict very small cross sections at small angles for the $1p_{1/2} \rightarrow 2p_{3/2}$ transitions (1.66 MeV in ⁴⁹V and 2.41 MeV in ⁵¹V) just as they did for the similar ⁶²Ni \rightarrow ⁶³Cu ground state transition. The DWBA calculations for all potentials predict for larger cross sections for the $1p_{1/2} \rightarrow 1f_{5/2}$ transition to the 2.19 MeV state of ⁴⁹V. The data do not support this strong configuration dependence.

D. Spectroscopic factors

Since the DWBA calculations discussed above have not produced generally good fits to the measured angular distributions, it is not at all clear how to extract spectroscopic factors or how to assess the implications of such factors once extracted. For the data which show a grazing angle maximum an appeal can be made to the well established result that fitting DWBA calculations to this maximum generally yields spectroscopic factors in good agreement with those derived from (³He, d) reaction data.⁶⁻⁹ Table II lists spectroscopic factors for all the transitions of this study. These have been extracted from the normalizations shown in Figs. 1-4 of the DWBA curves to the grazing angle regions of the measured angular distributions by using the relation¹³

$$\frac{d\sigma}{d\Omega_{\text{exp}}} = 2 \left(\frac{2J_{\text{fin}} + 1}{2J_{\text{init}} + 1} \right) (C^2S) \times \sum_l (2l+1) W^2(1 \frac{1}{2} l_f j_f; \frac{1}{2} l) \frac{d\sigma}{d\Omega_{l, \text{LOLA}}},$$

where l_f, j_f are the assumed orbital and total angular momentum of the transferred proton in the final nucleus and the spectroscopic factor of the $1p_{1/2}$ proton bound in the projectile has been set equal to 2. These spectroscopic factors are clearly in rather good agreement with those reported from (³He, d) investigations (also listed in Table II). The main exceptions to this statement arise from transitions to the $j=l-\frac{1}{2}$ states at 4.61 MeV in ²⁸Si and 2.19 MeV in ⁴⁹V. The full-finite-range calculation has been reported to eliminate such difficulties,⁶ but it appears to reduce but not com-

pletely solve the $j=l-\frac{1}{2}$ discrepancy in these cases.

Although the (¹⁶O, ¹⁵N) absolute spectroscopic factors depend significantly on the choice of optical potential for the DWBA calculations, there is a strong dependence (mentioned above) of the DWBA cross section on quite reasonable changes in the radius and diffuseness of the Woods-Saxon well used to calculate the form factor. This eliminates any possibility of favoring one optical potential over others on the basis of the absolute spectroscopic factors of Table II.

The beam energy variations of the spectroscopic factors in Table II are not large (the absolute spectroscopic factors for 36 MeV ²⁶Mg \rightarrow ²⁷Al transitions should probably be ignored here since severe kinematic shifts of the focal plane of the split-pole spectrograph made it impossible to extend these angular distributions to angles as large as the grazing angle maximum). The ²⁷Al \rightarrow ²⁸Si ground state transitions are sufficiently well fitted by the potential C calculations that the factor of 2 variations of this spectroscopic factor with beam energy are probably significant. But certainly the present data do not show any systematic as striking as the smooth factor of ~ 5 decrease observed over a 20 MeV beam energy variation for the ²⁴Mg and ²⁸Si(¹⁶O, ¹²C) reactions.³ On the other hand, the (¹⁶O, ¹²C) angular distributions do not show a grazing angle maximum — they show strong diffraction oscillations about an average value that decreases exponentially with increasing angle, and the DWBA analysis of these data gave greatest weight to fitting the small angle cross sections. Clearly, normalizing to the small angle structure seen in (¹⁶O, ¹⁵N) transitions would result in wildly varying energy dependences of spectroscopic factors.

E. m state dependences

As the above discussion indicates, the success or failure of the DWBA in fitting (¹⁶O, ¹⁵N) angular distributions seems to depend in a complicated way on several factors. Transfer into a $j=l-\frac{1}{2}$ orbital yielded anomalous spectroscopic factors in both observed cases — along with anomalous angular distribution shapes. Transitions with very unfavorable Q values also appear to exhibit small angle cross sections that are not generally reproduced by the DWBA. The one set of well fitted angular distributions with favorable Q values and a large range of bombarding energies shows a fluctuation in spectroscopic factor reminiscent of but smaller than that reported for the ²⁴Mg, ²⁸Si(¹⁶O, ¹²C) cases.³ The (¹⁶O, ¹²C) results may provide a useful insight here. The angular distributions for the (¹⁶O, ¹²C) ground state transi-

tions could be fitted quite well with DWBA calculations using a potential very like potential C — despite a mismatch of several units of angular momentum. But the (^{16}O , ^{12}C) $l=2$ angular distributions showed more oscillatory structure than the DWBA calculations could predict. The relatively featureless DWBA $l=2$ patterns arose from an averaging over roughly equal contributions from the various allowed m values. It is tempting to attribute some of the DWBA failure to a misassessment of the relative populations of different m substates which becomes progressively more severe with angular momentum mismatch. Under such an assumption the mismatched (^{16}O , ^{12}C) ground state angular distributions could still be fitted because there is no mixing of m substates.

DWBA calculations for (^{16}O , ^{15}N) transitions have been reported¹ to favor $m=\pm l$ transitions over all other m substates — at least at small angles. This result also holds for the strong, well matched transitions in the present study, as can be seen from parts (a) and (c) of Fig. 8 where the m substate partial cross sections for two such calculations have been drawn together with their sums.

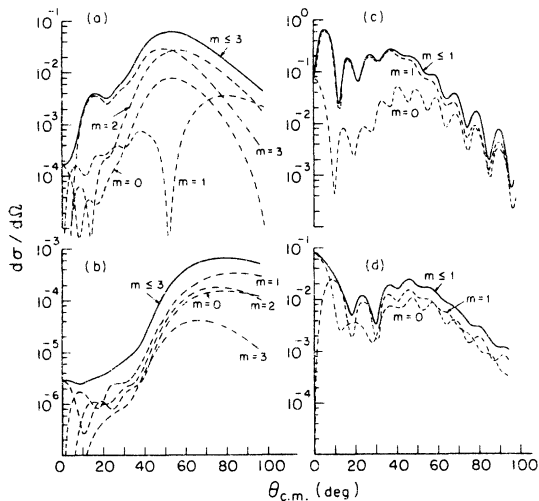


FIG. 8. Partial DWBA angular distributions are shown as dashed curves for the indicated projections m of transferred orbital angular momentum. The full DWBA angular distributions, incoherent sums of the partial angular distributions, are shown as solid curves. All calculations are for $^{27}\text{Al}(^{16}\text{O}, ^{15}\text{N})^{28}\text{Si}$ transitions. Assumed optical potentials, beam energies, and residual states in ^{28}Si are as follows: (a) ground state, 36 MeV, potential set A from Table I with exit channel imaginary diffuseness set to 0.6 fm as discussed in the text; (b) same as case (a) except the Q value and final state binding energy were arbitrarily changed to give a final state excitation energy of 7 MeV; (c) 1.78 MeV 2^+ state, 42 MeV, potential set C; and (d) 4.61 MeV 4^+ state, 42 MeV, potential set C.

However, Fig. 8 also shows two cases where the $m=\pm l$ partial cross section does not dominate; in part (b) of the figure the Q value of the $l=3$ transition of part (a) has arbitrarily been driven far from the optimum value and the relative contributions from the different m substates can be seen to have been strongly modified. It has previously been reported that the DWBA-predicted grazing angle maximum moves to larger angles with increasing residual excitation energy much more rapidly than the maximum of the data.^{8,9,12} It is interesting to note in Fig. 8(b) that the maximum of the $m=\pm 3$ angular distribution shifts much less severely with excitation energy and the anomalous DWBA peak shift appears to come from the rapidly increasing emphasis on contributions from $|m|<3$ substates.

Another long-standing and related puzzle in applying DWBA analysis to (^{16}O , ^{15}N) angular distributions has arisen from the need to modify the exit channel optical potential to bring the DWBA grazing angles into agreement with the grazing angles of the strong, well matched transitions.^{4,8,9} Figure 8(a) shows a calculation for such a transition with the standard prescription applied (exit channel imaginary diffuseness increased by 0.1 fm). The only substantial effect of this modification was to reduce the $m=2$ partial cross section by $\sim 15\%$ relative to that from $m=3$. Since $m=2$ dominates at angles larger than the grazing angle the effect is to reduce the angle of the maximum.

Part (d) of Fig. 8 shows m state contributions for the poorly fitted $1p_{1/2} - 1d_{3/2}$ transfer to the 4.61 MeV state of ^{28}Si . Neither the $m=0$ nor the $m=\pm 1$ contribution dominates in this case and the $|m|=l=1$ calculation would in fact give a somewhat better fit to the experimental data than does the full calculation. On the other hand, most of the poorly fitted angular distributions shown in Figs. 1–4 do not resemble the corresponding DWBA $m=\pm l$ partial cross sections much more than they resemble the full calculations. The difference noted above between DWBA angular distribution predictions for $j=l+\frac{1}{2}$ and $j=l-\frac{1}{2}$ cases does not appear to arise only from a relative enhancement of $|m|<l$ contributions in the $j=l-\frac{1}{2}$ case; rather, the dominant effects in the DWBA calculations arise from changes in the shapes of the individual partial angular distributions themselves.

It is difficult to assess the significance of the apparent need to modify the DWBA-predicted alignment of the transferred nucleon. Clearly one possibility is a breakdown in the assumption of a direct one-step mechanism. This possibility is especially favored by the obvious strong dependence on Q value since it is precisely when the normal direct transfer is disfavored that multi-step contamination can become most evident.²⁵

However, it may not be necessary to invoke higher order processes to understand the transitions presented herein; it was seen above that plausible changes in optical potential parameters can result in significant changes of alignment. Much recent attention has focused on proper approaches to the heavy ion optical potential²⁶ and it may soon be possible to fashion reliable optical potentials which account properly for absorption at and just inside the nuclear surface. Improvements in the scattering wave functions would be especially important for unfavored Q value transitions since calculations for these transitions are not generally dominated by contributions from any one entrance channel partial wave but rather rely on accurate accounting of small contributions from many partial waves.

IV. SUMMARY AND CONCLUSIONS

The ($^{16}\text{O}, ^{15}\text{N}$) angular distributions discussed above (1) exhibit shapes varying from smooth "bell" shapes to strong oscillations about a forward-peaked envelope and (2) are derived from transitions which span a wide range in Q value, bombarding energy, and orbital angular momentum transfer. The full-finite-range DWBA analysis provides an excellent account of the data only for bombarding energies well above the Coulomb barrier and Q values near the optimum value. While the $^{27}\text{Al} - ^{28}\text{Si}$ transitions (which span the largest range of bombarding energy of this data set) exhibit factor of ~ 2 fluctuations in absolute spectroscopic factor, there is no evidence for a smooth, systematic, bombarding-energy variation of ($^{16}\text{O}, ^{15}\text{N}$) absolute spectroscopic factors as was the case for Mg, Si($^{16}\text{O}, ^{12}\text{C}$)Si, S transitions.³ The ($^{16}\text{O}, ^{15}\text{N}$) spectroscopic factors appear to be in rather good agreement with ($^3\text{He}, d$) results, pro-

vided the DWBA predictions are normalized to the data at the grazing angle and the poor fit to small angle structure is ignored.

It is difficult to assess whether the failures of the present DWBA analysis indicate a breakdown in the one-step-direct-transfer mechanism assumptions or a need for more realistic channel wave functions. Certainly multistep processes can be expected to disturb the DWBA analysis most severely when the direct amplitudes become small — as in unfavored Q value and low-bombarding-energy cases. But the generally reasonable spectroscopic factors which result from DWBA analyses and the surprising success of simple semiclassical direct reaction calculations in predicting the bombarding-energy systematics of some reactions³ argue for the efficacy of the one-step-direct mechanism.

An examination of the effects on the full DWBA angular distribution of varying the relative contributions of different m substates raises intriguing possibilities for understanding the failures of the present DWBA approach. The success of the DWBA in predicting $l=0$ angular distribution shapes for ($^{16}\text{O}, ^{12}\text{C}$) transitions³ (even for cases with very unfavorable Q values), the failures of the DWBA which have been ascribed to poor $m=0, 1$ admixtures in $l=1$ transitions,¹¹ and the well-known anomalous shift in the DWBA predicted grazing angle with changing Q value^{8,9,12} (which is seen above to arise from an extreme change in relative contributions from different m substates) all indicate that normal DWBA calculations predict an incorrect alignment of transferred angular momentum. Earlier DWBA analyses^{8,9,12} which employed an arbitrary modification of the exit channel optical potential appear to have adjusted the DWBA-predicted grazing angle through a modification of this alignment.

*Supported by National Science Foundation.

¹M. J. Schneider, C. Chasman, E. H. Auerbach, A. J. Baltz, and S. Kahana, *Phys. Rev. Lett.* **31**, 320 (1973); C. Chasman, S. Kahana, and M. J. Schneider, *ibid.* **31**, 1074 (1973); S. Kahana, in *Proceedings of the International Conference on Reactions between Complex Nuclei, Nashville, 1974*, edited by R. L. Robinson, F. K. McGowan, J. B. Ball, and J. H. Hamilton (North-Holland, Amsterdam/American Elsevier, New York, 1974), p. 189.

²J. B. Ball, O. Hansen, J. S. Larsen, D. Sinclair, and F. Videbaek, *Nucl. Phys.* **A244**, 341 (1975).

³J. C. Peng, J. V. Maher, W. Oelert, D. A. Sink, C. M. Cheng, and H. S. Song, *Nucl. Phys.* **A264**, 312 (1976), and references contained therein.

⁴Y. Eisen, H. T. Fortune, W. Henning, D. G. Kovar,

S. Vigdor, and B. Zeidman, *Phys. Rev. C* **13**, 699 (1976).

⁵M.-C. Lemaire, M. C. Mermaz, H. Sztark, and A. Consolo, *Phys. Rev. C* **10**, 1103 (1974); P. Braun-Munzinger, W. Bohne, C. K. Gelbke, W. Grochulski, H. L. Horney, and H. Oeschler, *Phys. Rev. Lett.* **31**, 1423 (1973).

⁶R. M. DeVries, *Phys. Rev. C* **8**, 951, 1542 (1973); R. M. DeVries, G. R. Satchler, and J. G. Cramer, *Phys. Rev. Lett.* **32**, 1377 (1974).

⁷K. S. Low and T. Tamura, *Phys. Rev. C* **11**, 789 (1975), and references contained therein.

⁸H. J. Korner, G. C. Morrison, L. R. Greenwood, and R. H. Siemssen, *Phys. Rev. C* **7**, 107 (1973).

⁹J. V. Maher, K. A. Erb, and R. W. Miller, *Phys. Rev. C* **7**, 651 (1973).

- ¹⁰D. Sinclair, Phys. Lett. 53B, 54 (1974); P. R. Christensen, Ole Hansen, J. S. Larsen, D. Sinclair, and F. Videbaek, Phys. Lett. 45B, 107 (1973); M. Conjeaud, S. Harar, E. F. DaSilveira, and C. Volant, Nucl. Phys. A250, 182 (1975).
- ¹¹P. D. Bond, C. Chasman, J. D. Garrett, C. K. Gelbke, Ole Hansen, M. J. LeVine, A. Z. Schwarzschild, and C. E. Thorn, Phys. Rev. Lett. 36, 300 (1976).
- ¹²T. J. Lewis, G. H. Wedberg, J. C. Peng, J. L. Ricci, C. M. Cheng, and J. V. Maher, Phys. Rev. C 8, 678 (1973).
- ¹³Code LOLA, R. M. DeVries (unpublished) using formalism of N. Austern, R. M. Drisko, E. Halbert, and G. R. Satchler, Phys. Rev. 133, B3 (1964); also see Ref. 6 and 7.
- ¹⁴R. H. Siemssen, Argonne National Laboratory Report No. ANL-7837, 1971 (unpublished), p. 145.
- ¹⁵W. Henning, Y. Eisen, H. T. Fortune, D. G. Kovar, and B. Zeidman (unpublished).
- ¹⁶M. J. Schneider, J. V. Maher, T. J. Lewis, J. C. Peng, C. M. Cheng, and H. S. Song, Bull. Am. Phys. Soc. 19, 503 (1974).
- ¹⁷Optical model calculations were performed with the codes GENOA (F.G. Perey) and ABACUS (E.H. Auerback).
- ¹⁸U. C. Voos, W. von Oertzen, and R. Bock, Nucl. Phys. A135, 207 (1969), and references contained therein.
- ¹⁹M.-C. Lemaire, M. C. Mermaz, H. Sztark, and A. Consolo, in *Proceedings of the International Conference on Reactions between Complex Nuclei, Nashville, 1974*, edited by R. L. Robinson, F. K. McGowan, J. B. Ball, and J. H. Hamilton (see Ref. 1), Vol. 1, p. 21.
- ²⁰P. J. A. Buttle and L. J. B. Goldfarb, Nucl. Phys. A176, 299 (1971).
- ²¹J. P. Schiffer, H. J. Körner, R. H. Siemssen, K. W. Jones, and A. Schwarzschild, Phys. Lett. 44B, 47 (1973).
- ²²E. Newman, K. S. Toth, and A. Zucker, Phys. Rev. 132, 1720 (1963).
- ²³R. W. Barnard and G. D. Jones, Nucl. Phys. A108, 641 (1968).
- ²⁴A. J. Baltz, P. D. Bond, J. D. Garrett, and S. Kahana, Phys. Rev. C 12, 136 (1975), and references contained therein.
- ²⁵K. S. Low, T. Tamura, and T. Udagawa, Report (unpublished); K. Yagi, D. L. Hendrie, L. Kraus, C. F. Maguire, J. Mahoney, D. K. Scott, Y. Terrien, T. Udagawa, K. S. Low, and T. Tamura, Phys. Rev. Lett. 34, 96 (1975).
- ²⁶G. R. Satchler, Phys. Lett. 59B, 121 (1975); 58B, 408 (1975); D. M. Brink and N. Rowley, Nucl. Phys. A219, 79 (1974); P. J. Moffa, C. B. Dover, and J. P. Vary, Phys. Rev. C 13, 147 (1976); and references contained therein.